Available online at www.sciencedirect.com

ScienceDirect

Mendeleev Commun., 2024, **34**, 715–717

Mendeleev Communications

Catalytic activity of MoO_3:V_2O_5 mixed oxides towards oxidation reactions: the nature of catalytic centers

Tatyana V. Sviridova,[a] Lubov Yu. Sadovskaya,[a] Olga V. Matrosova,[b] Marina V. Vishnetskaya,[b] Alexander I. Kokorin[c,d,e] and Dmitry V. Sviridov*[a]

[a] *Department of Chemistry, Belarusian State University, 220006 Minsk, Belarus. E-mail: sviridov@bsu.by*
[b] *National University of Oil and Gas 'Gubkin University', 119991 Moscow, Russian Federation*
[c] *N. N. Semenov Federal Research Center for Chemical Physics, Russian Academy of Sciences, 119991 Moscow, Russian Federation*
[d] *G. V. Plekhanov Russian University of Economics, 117997 Moscow, Russian Federation*
[e] *Infochemistry Scientific Center, ITMO University, 191002 St. Petersburg, Russian Federation*

DOI: 10.1016/j.mencom.2024.09.029

Singlet oxygen emission and peroxide generation at the surface of molybdenum–vanadium oxides evidenced that the catalytic activity of a MoO_3:V_2O_5 mixed oxide at 70–175 °C was governed by the formation of peroxo groups in the interaction of molecular oxygen with adjacent V^{IV} surface centers; the thermolysis of these groups yielded singlet oxygen capable of oxidizing selectively alcohols to aldehydes.

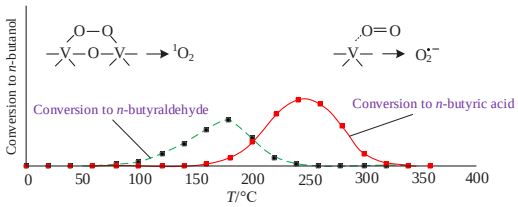

Keywords: molybdenum–vanadium mixed oxides, singlet oxygen, catalysis, oxidation, peroxo groups, clusterization of redox centers.

Mixed molybdenum–vanadium oxides are promising catalysts for oxygen atom transfer reactions including selective oxidation of alkanes,[1,2] alcohols,[3] benzene, toluene,[4–7] and thiophene[5,8,9] with the use of molecular oxygen as an environmentally friendly oxidizing agent. The catalytic behavior of mixed molybdenum–vanadium oxides is governed by generation of electronically excited oxygen species $^1\Delta_gO_2$ (so-called singlet oxygen) occurring at temperatures higher than 300 °C with lattice oxygen involved in this process.[3,10–12] The products of these catalytic reactions are often not identical to those obtained in oxidation reactions involving the conventional triplet form of molecular oxygen.[13,14] Moreover, a recently discovered effect of the low-temperature emission of singlet oxygen inherent in mixed molybdenum–vanadium oxides[10,15] opens fresh opportunities for selective low-temperature oxidation of organic compounds. In these catalytic processes, the redox centers V^V/V^{IV} and Mo^{VI}/Mo^V at the catalyst surface ensure activation of triplet oxygen molecules,[15,16] but the mechanism of catalytic oxidation with mixed molybdenum–vanadium oxides and the nature of active intermediates involved in these reactions remain unclear. On the other hand, it was found recently that the interaction of molecular oxygen with non-equilibrium Mo^V and V^{IV} centers produced in illuminated TiO_2/MoO_3 and TiO_2/MoO_3:V_2O_5 photocatalysts yielded hydrogen peroxide molecules, which can be desorbed from the photocatalyst surface.[17] Thus, there is a unifying mechanism responsible for the activation of molecular oxygen and stabilization of intermediate species at the molybdenum–vanadium catalyst surface through the interaction of intermediates with surface unsaturated-coordination centers coinciding with redox centers. The aim of this study was to examine the nature of surface centers responsible for the catalytic behavior of mixed molybdenum–vanadium oxides in the test reaction of *n*-butanol oxidation to *n*-butyraldehyde (the oxidation product in the case of singlet oxygen).

The molybdenum–vanadium oxides [$x$$MoO_3$:$(1 - x)$$V_2O_5$] with x = 0.25, 0.5, 0.75, and 0.90 were prepared by evaporation of a mixed aqueous solution of ammonium metavanadate (NH_4VO_3, 99%, Sigma Aldrich) and ammonium heptamolybdate [$(NH_4)_6Mo_7O_{24}$, 83%, Sigma Aldrich] followed by calcination of the precipitate at 450 °C for 5 h.

X-ray powder diffraction analysis† showed that the solid-state synthesis of $x$$MoO_3$:$(1 - x)$$V_2O_5$ (x = 0.25–0.75) mixed oxides yielded a monoclinic $(Mo_{0.3}V_{0.7})_2O_5$ solid solution as the main phase with an impurity of rhombohedral V_2O_5. Introduction of molybdenum ions into the lattice of vanadium oxide resulted in the formation of excess V^{IV} centers, which is consistent with partial reduction of resultant oxide composite.

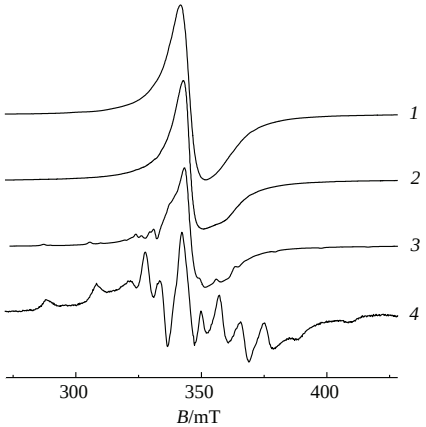

Figure 1 EPR spectra of V^{IV} ions in $x$$MoO_3$:$(1 - x)$$V_2O_5$ mixed oxides at 77 K : x = (*1*) 0.25, (*2*) 0.5, (*3*) 0.75, and (*4*) 0.9.

† Powder X-ray diffraction analysis of $x$$MoO_3$:$(1 - x)$$V_2O_5$ was performed with an Empyrean diffractometer (PANalytical) using Cu$K\alpha$ radiation. The diffractograms were analyzed using the X'pert Highscore Plus software.

Intense EPR signals from V^{IV} paramagnetic centers (PCs) were observed in $xMoO_3:(1-x)V_2O_5$ mixed oxides (Figure 1).‡ Paramagnetic Mo^{V} species, if they were, were masked by a huge V^{IV} spectrum. Figure 1 shows that the shape of the spectrum changed considerably with the molybdenum content, whereas the spatial structure of PCs was similar to that of vanadyl complexes.[5] An increase of the vanadium oxide content from 10 to 75 mol% transformed a typical anisotropic eight-component EPR spectrum ($I_V = 7/2$, where I_V is the ^{51}V nuclear spin) (Figure 1, curve *4*) into a broad anisotropic single line (Figure 1, curves *1* and *2*), which is indicative of the formation of magneto-concentrated associates with a high local PC concentration along with the presence of isolated centers (about 20–30 mol%). Thus, an increase in vanadium oxide loading resulted in an increase in the concentration of magneto-concentrated associates. At a vanadium oxide concentration of 50 mol%, almost all paramagnetic vanadium ions occurred in these associates, giving rise to strong spin–exchange and dipole–dipole interaction between V^{IV} PCs and, hence, to singletization of the EPR spectrum (Figure 1, curves *1* and *2*). The double integration of EPR spectra showed that vanadium ions in the sample occurred mostly in a paramagnetic state [only ~30% of vanadium ions remained in the diamagnetic V^{V} state]. The autoreduction of vanadium ions in $MoO_3:V_2O_5$ solid solutions was discussed in detail previously.[9]

The oxidation of *n*-butanol was carried out in a temperature range of 50–350 °C using finely divided $MoO_3:V_2O_5$ powder as a catalyst mixed with quartz powder in a ratio of 1:12 and deposited onto the fixed bed inside a flow reactor. The reaction products were analyzed chromatographically.§ The emission of $^1\Delta_gO_2$ was investigated in the above temperature range using a specially developed chemiluminescence technique.¶,[10]

Figure 2 shows that the oxidation of *n*-butanol at the surface of the $MoO_3:V_2O_5$ mixed oxide led to a limited number of oxidation products including *n*-butyraldehyde, butyric acid, and CO_x; butyraldehyde was the only oxidation product in a temperature range of 70–175 °C. At higher temperatures, the yield of the aldehyde decreased and butyric acid prevailed among the oxidation products. On the other hand, it is evident from the temperature dependence of the yield of singlet oxygen that the temperature range where the $^1\Delta_gO_2$ emission was observed was identical to the temperature range where the oxidation of *n*-butanol to *n*-butyraldehyde prevailed. This allowed us to suggest that the low-temperature oxidation of *n*-butanol to butyraldehyde occurred *via* activation of oxygen molecules at the catalyst surface yielding a singlet form of dioxygen, which behaved as a selective oxidation agent.

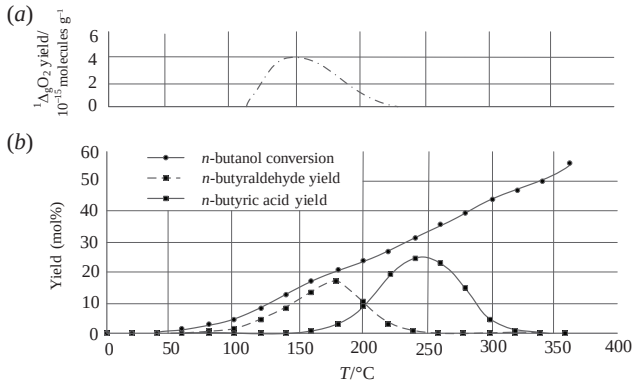

Figure 2 Temperature dependences of (*a*) $^1\Delta_gO_2$ emission and (*b*) *n*-butanol oxidation efficiency for $xMoO_3:(1-x)V_2O_5$, $x = 0.25$.

The emission of singlet oxygen (Figure 2) resulted from the thermolysis of peroxo groups[11] formed at the $MoO_3:V_2O_5$ catalyst surface due to interaction of oxygen molecules with V^{IV} centers. To study reaction intermediates at the surface of $MoO_3:V_2O_5$, we used thin films of a $MoO_3:V_2O_5/TiO_2$ composite†† permitting modulation of the concentration of V^{IV} centers by UV exposure (through the photocatalytic pumping leading to the injection of photoelectrons from TiO_2 into a $MoO_3:V_2O_5$ matrix). Since the energy level of a conduction band of V_2O_5 lies above the energy level corresponding to a MoO_3 conduction band (but at a lower energy as compared to the conduction band position of TiO_2),[17,19,20] the trapping of photoelectrons occurred *via* a cascade mechanism.

Figure 3 shows that the pre-exposed $MoO_3:V_2O_5/TiO_2$ film generated luminescence in contact with a luminol solution containing Fe^{2+} ions due to interaction of luminol molecules with hydroxyl radicals produced *via* Fe(II)-assisted conversion of photogenerated peroxo species (Fenton reaction).‡‡ However, chemiluminescence was not observed in the absence of Fe^{2+} ions (Figure 3). Thus, in the $MoO_3:V_2O_5/TiO_2$ composite, the titania-assisted photoproduction of O_2^- species (which, along with hydroxyl radicals, are responsible for photooxidation activity of titania[18]) was negligible and photogenerated electrons were mostly trapped in the $MoO_3:V_2O_5$ mixed oxide. Oxidation of resultant V^{IV} centers at the $MoO_3:V_2O_5$ surface by molecular oxygen led to the formation of peroxo species, which underwent further hydrolysis, yielding free hydrogen peroxide due to high hydrophilcity inherent in $MoO_3:V_2O_5$.[17]

The detected *n*-butanol oxidation products suggested that peroxo species generated at the $MoO_3:V_2O_5$ mixed oxide surface

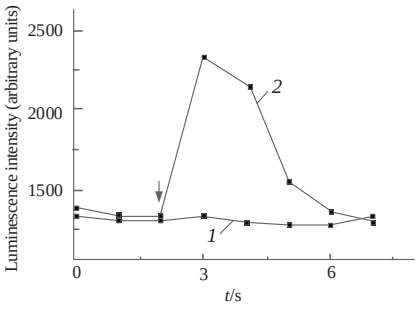

Figure 3 Time dependence of the luminescence intensity for the UV-exposed $MoO_3:V_2O_5/TiO_2$ film. The arrow corresponds to the moment of the insertion of (*1*) luminol or (*2*) luminol + Fe^{II} solution.

‡ The X-band EPR spectra were recorded at 77 K using a Bruker EMX-8 spectrometer. The microwave power was 0.1 mW with a modulation frequency of 100 kHz. The PC concentration was evaluated by the double integration of the EPR spectrum using a $CuCl_2·2H_2O$ crystal with a known number of spins as a reference standard.

§ The liquid products of *n*-butanol oxidation were analyzed on a Cambridge GC-95 chromatograph equipped with a capillary column (FFAP phase, 50 m); the gaseous products were identified using a Crystatallux 400M chromatograph with an activated carbon packed column.

¶ The amount of desorbed singlet oxygen was evaluated from the chemiluminescence intensity of methoxymethyl-10′-9,9′-biacrylidene used as a probing dye.

†† The $MoO_3:V_2O_5/TiO_2$ composite was prepared by suspending $0.25MoO_3:0.75V_2O_5$ particles (0.5–0.7 μm in size) in a TiO_2 colloid (obtained through hydrolysis of $TiCl_4$, yielding anatase crystallites with a mean size of 4 nm). The resultant suspension was deposited onto a glass substrate by pulverization and calcined at 200 °C. The TiO_2 loading in the obtained $MoO_3:V_2O_5/TiO_2$ composite film was 20 wt%; the film thickness was about 1.5 μm.

‡‡ In these experiments, the $MoO_3:V_2O_5/TiO_2$ film was exposed to UV light for 30 min in the cuvette of a Fluoromax-2 spectrofluorometer (Horiba). Immediately after exposure, the cuvette was filled with a luminol solution (4 g dm^{-3}) containing 10^{-4} M Fe_2SO_4 and the time dependence of chemiluminescent signals was measured.

as a result of binding oxygen molecules with adjacent V^{IV} centers behaved as active intermediates in the low-temperature oxidation reaction of aliphatic alcohols. This binding of oxygen molecules was facilitated by clusterization of V^{IV} centers in $MoO_3:V_2O_5$, which manifested itself in the pronounced anisotropy and partial singletization of the EPR signal (Figure 1), indicative of strong spin–spin interactions between vanadium paramagnetic centers. The clusterization was facilitated by structural peculiarities of a $(Mo_{0.3}V_{0.7})_2O_5$ phase consisting of layers[§§] built from closely packed $[MeO_6]$ octahedrons.

Thus, the dynamic behavior of active intermediates responsible for the oxidation properties of a $MoO_3:V_2O_5$ catalyst can be represented as follows: At room temperature, the peroxo groups produced on the catalyst surface due to interaction with molecular oxygen converted into hydrogen peroxide, which was desorbed from the surface. In a temperature range of 70–175 °C, the thermolysis of these peroxo groups was accompanied by emission of singlet oxygen responsible for selective oxidation of *n*-butanol to *n*-butyraldehyde. However, at higher temperatures, the generation of vacancies at the catalyst surface became possible, and readsorption of oxygen on these vacancies *via* single-center bonding yielded superoxide intermediates capable of oxidizing *n*-butanol to *n*-butyric acid.

This work was performed within the framework of the State Program of Scientific Research of Belarus (state registration no. 20212675) and supported by the Program of Fundamental Research of the Russian Federation (registration no. 122040500068-0).

Online Supplementary Materials

Supplementary data associated with this article can be found in the online version at doi: 10.1016/j.mencom.2024.09.029.

[§§] For an electron microscopy image (Figure S1) of the layered structure of $MoO_3:V_2O_5$, see Online Supplementary Materials.

References

1 V. V. Pushkarev, V. I. Kovalchuk and J. L. d'Itri, *J. Phys. Chem. B*, 2004, **108**, 5341.
2 P. A. Vakhrushin, T. V. Sviridova, M. V. Vishnetskaya, D. V. Sviridov and A. I. Kokorin, *Russ. J. Phys. Chem. B*, 2012, **6**, 711 (*Khim. Fiz.*, 2012, **31**, 28).
3 V. I. Sobolev and K. Yu. Koltunov, *Kinet. Catal.*, 2015, **56**, 343.
4 T. Andersson and S. Lars, *J. Catal*., 1986, **98**, 138.
5 A. Satsuma, A. Hattory, K. Mizutani, A. Furuta, A. Miyamoto, T. Hattory and Y. Murukami, *J. Phys. Chem*., 1989, **93**, 1484.
6 E. Wenda and A. Bielanski, in *Molybdenum: Characteristics, Production and Applications*, eds. M. Ortiz and T. Herrera, Nova Science Publishers, New York, 2012, pp. 215–225.
7 M. J. Davies, *Photochem. Photobiol. Sci.*, 2004, **3**, 17.
8 M. Kasha and D. E. Brabham, in *Singlet Oxygen*, eds. H. H. Wasserman and R. W. Murray, Academic Press, New York, 1979, pp. 1–33.
9 T. V. Sviridova, A. A. Antonova, E. V. Boikov, M. V. Vishnetskaya, D. V. Sviridov and A. I. Kokorin, *Russ. J. Phys. Chem. B*, 2013, **7**, 118 (*Khim. Fiz.*, 2013, **32**, 29).
10 O. V. Matrosova, Y. N. Rufov and M. V. Vishnetskaya, *Russ. J. Phys. Chem. A*, 2010, **8**4, 2187 (*Zh. Fiz. Khim*., 2010, **84**, 2387).
11 L. G. Possato, W. H. Cassinelli, C. I. Meyer, T. Garreto, S. H. Pulcinelli, C. V. Santilli and L. Martins, *Appl. Catal., A*, 2017, **532**, 1.
12 S. Stoll and A. Schweiger, *J. Magn. Reson.*, 2006, **178**, 42.
13 M. Iwamoto and J. H. Lunsford, *J. Phys. Chem.*, 1980, **84**, 3079.
14 V. I. Sobolev and K. Yu. Koltunov, *Appl. Catal., A*, 2014, **476**, 197.
15 S. Guimond, M. Abu Haija, S. Kaya, J. Lu, J. Weissenriwder, S. Shaikhutdinov, H. Kuhlenbeck, H.-J. Freund, J. Döbler and J. Sauer, *Top. Catal.*, 2006, **38**, 117.
16 M. Abu Haija, S. Guimond, Y. Romanyshyn, A. Uhl, H. Kuhlenbeck, T. K. Todorova, M. V. Ganduglia-Pirovano, J. Döbler, J. Sauer and H.-J. Freund, *Surf. Sci*., 2006, **600**, 1497.
17 T. V. Sviridova, L. Yu. Sadovskaya, E. A. Konstantinova, N. A. Belyasova, A. I. Kokorin and D. V. Sviridov, *Catal. Lett.*, 2019, **149**, 1147.
18 K. Ishibashi, A. Fujishima, T. Watanabe and K. Hashimoto, *J. Phys. Chem. B*, 2000, **104**, 4934.
19 E. V. Kytina, E. R. Parkhomenko, E. A. Nazarova and E. A. Konstantinova, *Dokl. Phys.*, 2021, **66**, 191 (*Dokl. Ross. Akad. Nauk. Fizika, Tekh. Nauki*, 2021, **499**, 8).
20 E. A. Konstantinova, A. A. Minnekhanov, E. V. Kytina and G. V. Trusov, *JETP Lett.*, 2020, **112**, 527 (*Pis'ma ZhETF*, 2020, **112**, 562).

Received: 29th March 2024; Com. 24/7440